

# UC Irvine

## UC Irvine Previously Published Works

### Title

Targeted deletion of Kcne3 impairs skeletal muscle function in mice

### Permalink

<https://escholarship.org/uc/item/32n8d394>

### Journal

The FASEB Journal, 31(7)

### ISSN

0892-6638

### Authors

King, Elizabeth C  
Patel, Vishal  
Anand, Marie  
et al.

### Publication Date

2017-07-01

### DOI

10.1096/fj.201600965rr

### Copyright Information

This work is made available under the terms of a Creative Commons Attribution License, available at <https://creativecommons.org/licenses/by/4.0/>

Peer reviewed

## Targeted deletion of *Kcne3* impairs skeletal muscle function in mice

Elizabeth C. King,<sup>\*,1</sup> Vishal Patel,<sup>†,1</sup> Marie Anand,<sup>‡,§</sup> Xiaoli Zhao,<sup>†,2</sup> Shawn M. Crump,<sup>‡,§</sup> Zhaoyang Hu,<sup>‡,§</sup> Noah Weisleder,<sup>†,3,4</sup> and Geoffrey W. Abbott<sup>‡,§,5</sup>

<sup>\*</sup>Department of Pharmacology, Weill Medical College of Cornell University, New York, New York, USA; <sup>†</sup>Department of Physiology and Biophysics, University of Medicine and Dentistry of New Jersey–Robert Wood Johnson Medical School, Piscataway, New Jersey, USA; and <sup>‡</sup>Department of Pharmacology and <sup>§</sup>Department of Physiology and Biophysics, School of Medicine, University of California, Irvine, Irvine, California, USA

**ABSTRACT:** KCNE3 (MiRP2) forms heteromeric voltage-gated K<sup>+</sup> channels with the skeletal muscle-expressed KCNC4 (K<sub>v</sub>3.4) α subunit. KCNE3 was the first reported skeletal muscle K<sup>+</sup> channel disease gene, but the requirement for KCNE3 in skeletal muscle has been questioned. Here, we confirmed KCNE3 transcript and protein expression in mouse skeletal muscle using *Kcne3*<sup>-/-</sup> tissue as a negative control. Whole-transcript microarray analysis (770,317 probes, interrogating 28,853 transcripts) findings were consistent with *Kcne3* deletion increasing gastrocnemius oxidative metabolic gene expression and the proportion of type IIa fast-twitch oxidative muscle fibers, which was verified using immunofluorescence. The down-regulated transcript set overlapped with muscle unloading gene expression profiles (≥1.5-fold change; *P* < 0.05). Gastrocnemius K<sup>+</sup> channel α subunit remodeling arising from *Kcne3* deletion was highly specific, involving just 3 of 69 α subunit genes probed: known KCNE3 partners KCNC4 and KCNH2 (mERG) were down-regulated, and KCNK4 (TRAAK) was up-regulated (*P* < 0.05). Functionally, *Kcne3*<sup>-/-</sup> mice exhibited abnormal hind-limb clasp upon tail suspension (63% of *Kcne3*<sup>-/-</sup> mice ≥10-mo-old vs. 0% age-matched *Kcne3*<sup>+/+</sup> littermates). Whereas 5 of 5 *Kcne3*<sup>+/+</sup> mice exhibited the typical biphasic decline in contractile force with repetitive stimuli of hind-limb muscle, both *in vivo* and *in vitro*, this was absent in 6 of 6 *Kcne3*<sup>-/-</sup> mice tested. Finally, myoblasts isolated from *Kcne3*<sup>-/-</sup> mice exhibit faster-inactivating and smaller sustained outward currents than those from *Kcne3*<sup>+/+</sup> mice. Thus, *Kcne3* deletion impairs skeletal muscle function in mice.—King, E. C., Patel, V., Anand, M., Zhao, X., Crump, S. M., Hu, Z., Weisleder, N., Abbott, G. W. Targeted deletion of *Kcne3* impairs skeletal muscle function in mice. *FASEB J.* 31, 2937–2947 (2017). www.fasebj.org

**KEY WORDS:** K<sub>v</sub>3.4 · MiRP2 · myotonia · periodic paralysis · potassium channel

KCNE3, originally designated MinK-related peptide 2 (MiRP2), is a single transmembrane domain β subunit that forms heteromeric complexes with voltage-gated

potassium (K<sub>v</sub>) channel pore-forming α subunits (1, 2). KCNE3 converts K<sub>v</sub> channels formed by the K<sub>v</sub>3.4 (KCNC4) α subunit from supra- to subthreshold activating, which we previously suggested regulates skeletal myocyte excitability (3). The functional screening for KCNE3 partners in skeletal muscle that uncovered its interaction with K<sub>v</sub>3.4 was initiated by the discovery of 2 small pedigrees in which a human KCNE3 single-point mutation (G340A, encoding an R83H substitution in KCNE3 protein) correlated 100% with periodic paralysis, a potentially debilitating skeletal myopathy that presents with a wide range of severity and penetrance. Sequencing of 100 individuals without periodic paralysis failed to uncover the R83H mutation, suggesting against it being a common benign polymorphism (3).

These findings made KCNE3 the first potassium channel subunit associated with any skeletal muscle disease. However, the association between KCNE3-R83H and skeletal muscle disease was subsequently questioned, after others reported finding R83H carriers who did not exhibit symptoms of periodic paralysis (4, 5).

**ABBREVIATIONS:** BLAST, Basic Local Alignment Search Tool; EDL, extensor digitorum longus; GAPDH, glyceraldehyde phosphate dehydrogenase; K<sub>v</sub>, voltage-gated potassium; qPCR, quantitative PCR; RLE, relative log expression

<sup>1</sup> These authors contributed equally to this work.

<sup>2</sup> Current affiliation: Department of Physiological Sciences, Eastern Virginia Medical School, Norfolk, VA, USA.

<sup>3</sup> Current affiliation: Department of Physiology and Cell Biology, Davis Heart and Lung Research Institute, Ohio State University, Columbus, OH, USA.

<sup>4</sup> Correspondence: Department of Physiology and Cell Biology, Davis Heart and Lung Research Institute, Ohio State University, 473 W. 12th Ave., Columbus, OH 43210-1252, USA. E-mail: noah.weisleder@osumc.edu

<sup>5</sup> Correspondence: Department of Pharmacology and Department of Physiology and Biophysics, University of California, 360 Med Surge II, School of Medicine, Irvine, CA 92697, USA. E-mail: abbottg@uci.edu

doi: 10.1096/fj.201600965RR

This article includes supplemental data. Please visit <http://www.fasebj.org> to obtain this information.

More recently, studies on a *Kcne3*<sup>-/-</sup> mixed 129/SvJ-C57BL/6 mouse line confirmed the role of KCNE3 in mouse colon but failed to find evidence of a skeletal muscle role for KCNE3, although muscle fiber contractile force was not quantified in that study (6). Here, to address these discrepancies, we independently generated *Kcne3*<sup>-/-</sup> mice in a C57BL/6J-*Tyr*<sup>c-2J</sup>/J (C2J) background and examined their skeletal muscle composition and contractile function. We found that targeted deletion of the *Kcne3* gene in mice impairs skeletal muscle function, altering muscle contractility and myoblast electrical properties, and causing fiber-type switching and muscle transcriptome remodeling.

## MATERIALS AND METHODS

### Generation of *Kcne3* gene-targeted mice

All mice and rats were housed and utilized according to the *Guide for the Care and Use of Laboratory Animals* (National Institutes of Health, Bethesda, MD, USA) and Weill Medical College of Cornell University and University of California, Irvine animal care and use policies. *Kcne3*<sup>-/-</sup> C2J mice were generated and genotyped as we recently described (7).

### Real-time quantitative PCR

Mice were humanely killed by CO<sub>2</sub> asphyxiation. Muscle was extracted after death, flash frozen in liquid nitrogen, and stored at -80°C until use. Tissue samples were removed from -80°C and submerged for 8 h in RNAlater Ice (Ambion, Austin, TX, USA) at -20°C, then RNA extracted using the RNeasy Mini Kit (Qiagen, Germantown, MD, USA) after homogenization with a pestle grinder system (Thermo Fisher Scientific, Waltham, MA, USA). RNA yield and purity (*A*<sub>260</sub>/*A*<sub>280</sub>) were determined by NanoDrop 2000 (Thermo Fisher Scientific) spectrophotometer. RNA samples with *A*<sub>260</sub>/*A*<sub>280</sub> absorbance ratios between 1.80 and 2.10 were used for cDNA synthesis. cDNA was synthesized from 1 μg RNA using Quantitect Reverse Transcriptase (Qiagen). Template RNA was mixed with gDNA Wipeout Buffer (Qiagen) and incubated at 42°C for 2 min to remove genomic DNA. Quantitect reverse transcriptase containing an RNase inhibitor and Quantiscript RT Buffer (containing Mg<sup>2+</sup> and dNTPs) were added to the genomic DNA elimination reaction and incubated at 42°C for 15 min. The reverse transcription reaction was inactivated with 3-min incubation at 95°C.

Primer pairs for target gene *Kcne3* (GeneID 57442; National Center for Biotechnology Information, Bethesda, MD, USA; <https://www.ncbi.nlm.nih.gov/>) produced an amplicon of 143 bp; match position of the expected sequence is number 1 out of 1001 Basic Local Alignment Search Tool (BLAST) matches. Primer pairs for reference gene *glyceraldehyde phosphate dehydrogenase* (*Gapdh*; NCBI Gene ID 14433) produced an amplicon of 123 bp; match position of the expected sequence is number 1 of 251 BLAST matches. Primer sequences for quantitative PCR (qPCR) analysis were acquired from the Harvard Medical School PrimerBank: *Kcne3*, forward 5'-CTTTGCTCGATGGAAGGGGAC-3', and reverse 5'-GCTGTCTGTTGAGAGGCGTC-3'; *Gapdh* forward 5'-AGGTCGGTGTGAACGGATTG-3' and reverse 5'-TGTAGACCATGTAGTTGAGGTCA-3'. Primers (50 nM synthesis scale, desalted) were ordered from Thermo Fisher Scientific or from Sigma-Aldrich (St. Louis, MO, USA). qPCR analysis was performed on the Roche LightCycler 480 System (Roche, Basel, Switzerland) using LightCycler 480 SYBR Green I Master Mix and LightCycler 480 96-well white plates, or alternatively using the CFX Connect System, iTaq Universal

SYBR Green Supermix (Bio-Rad, Hercules, CA, USA), and 96-well clear plates. Thermocycling parameters were set according to manufacturer's protocols. Each reaction contained 5 μl of cDNA diluted 1:20, 1 μl of PCR-grade water, 2 μl of 10 μM forward primer, 2 μl 10 μM reverse primer, 10 μl 2× Master Mix containing dNTP mix, MgCl<sub>2</sub>, FastStart Taq DNA polymerase, reaction buffer, and SYBR Green I dye. Thermocycling parameters were as follows: for amplification, 1 cycle at 95°C (10 min); 45 cycles at 95°C (5 s), 68°C (5 s), and 72°C (25 s); for melting curve, 95°C (1 s), 65°C (1 s), and 95° (continuous); for cooling, 1 cycle 45°C (15 s).

Advanced relative quantification was used to obtain normalized changes in expression levels of *Kcne3* relative to control (*Gapdh*). Each sample was run in triplicate as a quality-control measure; triplicates varying from one another by more than 1 cycle were not considered. Melting curves were assessed for each reaction to verify the amplification of a single product. Primer pair amplification efficiency was established with calibration curves. Final analysis of statistical significance was calculated by 1-way ANOVA test (OriginLab, Northampton, MA, USA).

### Western blot analysis

Preparation of muscle protein samples and Western blot analysis approaches were conducted as previously described (8) with the following modification: the anti-KCNE3 rabbit polyclonal primary antibody (Alomone Labs, Tel Aviv, Israel) was used at 1:200 dilution. All other antibodies were used at concentrations that we previously published (9).

### Transcriptomics

Total RNA was prepared from homogenized gastrocnemius tissue from 3- to 7-mo-old female *Kcne3*<sup>+/+</sup> (*n* = 5) and *Kcne3*<sup>-/-</sup> (*n* = 6) mice using Trizol (Ambion) and RNeasy spin columns (Thermo Fisher Scientific), with all samples having a 260/280 ratio of 2.1 to 2.3. Amplified and biotinylated sense-strand DNA targets from the entire expressed transcriptome were then generated from the gastrocnemius RNA using the WT Expression Kit (Ambion) in conjunction with the GeneChip WT Terminal Labeling Kit (Affymetrix, Santa Clara, CA, USA) according to manufacturers' instructions, then hybridized for 20 h on MoGene-1\_1-st-v1 Array strips (Affymetrix); and washed, stained, and washed again with a GeneAtlas fluidics station (Affymetrix) before visualization and quantification of transcript expression on a GeneAtlas imaging station (Affymetrix). Each array contained 770,317 probes, interrogating 28,853 genes, giving an average of 26 probes per gene.

Statistical analysis of relative transcript expression and transcript annotation were performed using Partek Express software (Partek, Heidelberg, Germany), with an RMA import normalization algorithm (10) and the following Affymetrix library files: C:\Microarray Libraries\MoGene-1\_1-st-v1.r4.pgf; C:\Microarray Libraries\MoGene-1\_1-st-v1.r4.cf; C:\Microarray Libraries\MoGene-1\_1-st-v1.r4.qcc; C:\Microarray Libraries\MoGene-1\_1-st-v1.r4.mps; C:\Microarray Libraries\MoGene-1\_1-st-v1.na32.mm9.transcript.csv. None of the samples failed quality control using the default settings for Partek Express, which assess raw probe intensity mean, chip brightness, mean of median of absolute residuals obtained from the model fitted in the probe set summarization step (to assess how well the probes fit the model for a chip), absolute relative log expression (RLE) across all of the probe sets for each array (absolute RLE is obtained by calculating the absolute value of the log base 2 difference between the probe set signal estimate and the median of probe set signal estimates across all of the arrays; rle\_mean is then calculated by taking the mean of absolute RLEs for all of the probe sets on each array, with a low rle\_mean indicating low biologic

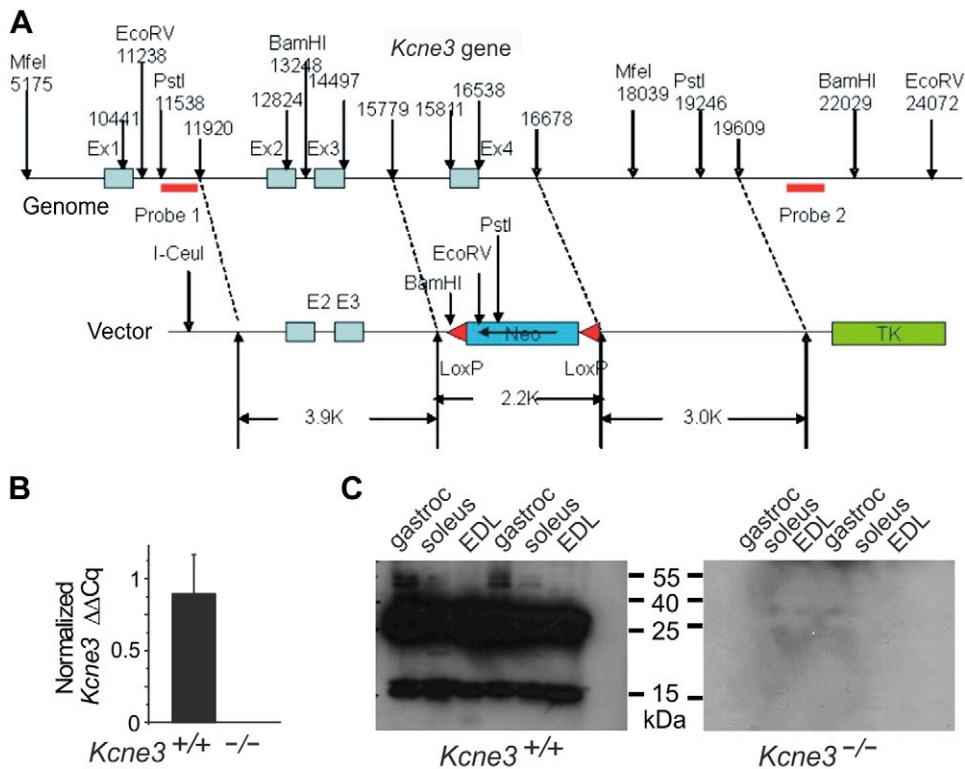


**Figure 1.** *Kcne3* transcript and protein are expressed in mouse skeletal muscle. **A)** *Kcne3* gene targeting strategy. **B)** qPCR quantification of *Kcne3* transcript normalized to *Gapdh*, isolated from *Kcne3*<sup>+/+</sup> and *Kcne3*<sup>-/-</sup> mouse gastrocnemius tissue. Values are means of 3 independent isolations, each performed in triplicate. Error bars indicate SEM. **C)** Western blot using anti-KCNE3 antibody of membrane preparations from different hind-limb skeletal muscle regions as indicated from 2 *Kcne3*<sup>+/+</sup> and 2 *Kcne3*<sup>-/-</sup> mice. Gastroc, gastrocnemius.

variability in replicates). Principle component analysis plot calculation (11) was performed with the correlation method. This is a 1-way ANOVA model using the method of moments (12):

$$\text{Model} : Y_{ij} = \mu + \text{Strain}_i + \epsilon_{ij}$$

where  $Y_{ij}$  represents the  $j$ th observation on the  $i$ th strain,  $\mu$  is the common effect for the whole experiment, and  $\epsilon_{ij}$  represents the random error present in the  $j$ th observation on the  $i$ th strain. The errors  $\epsilon_{ij}$  are assumed to be normally and independently distributed with mean 0 and SD  $\delta$  for all measurements. The following contrast was performed to compare genotypes (13): log transform status was base 2.0, and  $P$  value, log fold change, and ratios were calculated by geometric mean. The false discovery rate report (14) was generated by the Step Up method. Power analysis (15) was performed with the following parameters: comparison: *Kcne3*<sup>-/-</sup> vs. *Kcne3*<sup>+/+</sup>, effect size 1.25 to 3.0 by step 0.25, sample size 4 to 22 by step 2; significance 0.01; power 0.8. Analysis of gene ontologies and functional pathways altered by *Kcne3* deletion was performed using Pathway Analysis software (Elsevier, Amsterdam, The Netherlands), with default settings for significance.

## Histology and immunofluorescence

Mice were humanely killed by CO<sub>2</sub> asphyxiation. Gastrocnemius muscle was extracted after death. Tissue was fixed in 10% neutral buffered formalin, processed routinely, and embedded in paraffin. Sections were cut at 5- $\mu$ m intervals, placed on positively charged Superfrost slides, and stained with hematoxylin and eosin. For succinate dehydrogenase staining, gastrocnemius muscle was extracted and placed in base molds filled with optimal cutting temperature compound (frozen tissue matrix) and submerged in liquid nitrogen for 30 s. Sections were cut at 5- $\mu$ m intervals on a microtome cryostat and incubated in a solution containing 0.2 M phosphate buffer (pH 7.6), 0.1 M sodium succinate, and 1.2 mM nitro blue tetrazolium (Sigma-Aldrich) for 1 h at 37°C. Muscle fiber typing

was performed essentially as described previously by others (16) using myosin heavy chain immunostaining of frozen or deparaffinized paraffin-embedded adult female mouse gastrocnemius sections with the following monoclonal antibodies (Developmental Studies Hybridoma Bank, University of Iowa, Iowa): BA-58, type I (myosin heavy chain slow,  $\alpha$  and  $\beta$ ); SC-71, myosin heavy chain type IIa; BF-F3, myosin heavy chain type IIb; Alexa Fluor 488-conjugated donkey anti-mouse secondary antibody (Thermo Fisher Scientific) was used for fluorescent detection *via* an Olympus BX-51 microscope with Cell-Sens software (Olympus, Tokyo, Japan).

## Tail suspension

Hind-limb clasp during tail suspension has been used previously to assess the muscle stiffness and weakness associated with myotonia (17). Hind-limb clasp behavior was assessed by suspension of mice from the tail for 30 s. Mice were scored according to whether or not clasp behavior was observed within this time period.

## Contractility experiments

A custom *in vivo* muscle contractility device was used for assessment of change in muscle function associated with targeted deletion of *Kcne3* (18). Briefly, mice were anesthetized with isoflurane and the sciatic nerve stimulated with controlled electric pulses. The Achilles' tendon was attached to a motorized force transducer and the resulting force from contraction of the hind-limb muscle recorded. The following conditions were used for stimulation of muscle contraction: pulses per second, 140; pulse duration, 0.0001 s; trains per second, 0.8; train duration, 0.3 s. To measure the force/frequency relationship for each mouse tested, the pulses per second were changed to 20, 40, 60, 80, 100, 120, and 140 at 30-s intervals. For *in vitro* contractility studies, we used our previously published protocol (19).



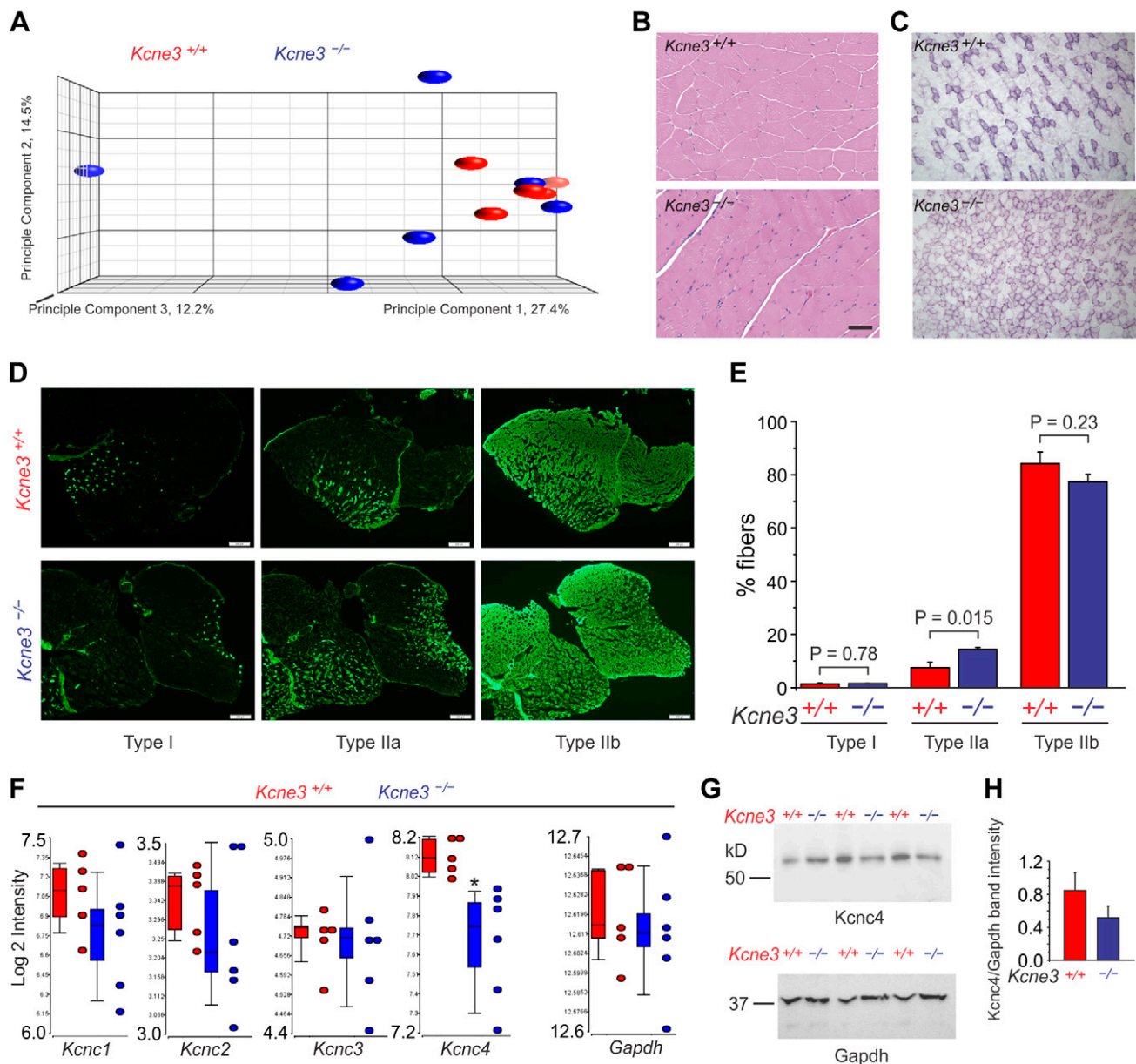


**Figure 2.** *Kcne3* deletion causes remodeling and muscle fiber-type switching. **A**) Principal component analysis of microarray data from gastrocnemius lysates of *Kcne3*<sup>+/+</sup> ( $n = 5$ ) and *Kcne3*<sup>-/-</sup> ( $n = 6$ ) mice. **B**) Hematoxylin and eosin–stained gastrocnemius sections from 10-mo-old *Kcne3*<sup>+/+</sup> and *Kcne3*<sup>-/-</sup> mice. Scale bar, 20  $\mu\text{m}$ . Representative of 3 sections from 4 mice per group. **C**) Succinate dehydrogenase stained gastrocnemius sections from 10-mo-old *Kcne3*<sup>+/+</sup> and *Kcne3*<sup>-/-</sup> mice. Scale bar, 40  $\mu\text{m}$ . Representative of 3 sections from 4 mice per group. **D**) Myosin heavy chain 2 (types I, IIa, and IIb) immunofluorescence-labeled adult female *Kcne3*<sup>+/+</sup> and *Kcne3*<sup>-/-</sup> mouse (10–12 mo) gastrocnemius sections. Scale bars, 200  $\mu\text{m}$ . Representative of 4–5 sections, 3 mice per genotype. **E**) Relative amounts of types I, IIa, and IIb fibers in gastrocnemius of *Kcne3*<sup>+/+</sup> and *Kcne3*<sup>-/-</sup> mice, quantified from images as in **D**; 4–5 sections per antibody per genotype, 3 mice per genotype. Total number of fibers evaluated is 150,336. **F**) Log<sub>2</sub> intensity of *Kcnc* family transcripts from microarray data as in **A**. \* $P < 0.05$  between genotypes. **G**) Exemplar Western blots for gastrocnemius lysates, mouse genotypes as indicated, probed with antibodies to Kcnc4 (K,3.4) and Gapdh. **H**) Mean Kcnc4 protein band intensity, normalized to Gapdh, from blots as in **G** ( $n = 4$ ).

### Myoblast electrophysiology

Skeletal muscle myoblasts were prepared from *Kcne3*<sup>+/+</sup> and *Kcne3*<sup>-/-</sup> mice as previously described (20). Nine mice per genotype were used, all of which were >12 mo of age. Spherical myoblasts from 3 separate preparations, each of which was pooled from gastrocnemius muscle from 3 mice, were used for each genotype. For whole-cell patch clamp, bath solution contained (mM) 135 NaCl, 5 KCl, 1.2 MgCl<sub>2</sub>, 5 HEPES, 2.5 CaCl<sub>2</sub>, and 10 D-glucose (pH 7.4). Pipettes were 2.1 to 3.5 M $\Omega$  resistance

when filled with intracellular solution containing (in mM) 10 NaCl, 117 KCl, 2 MgCl<sub>2</sub>, 11 HEPES, 11 EGTA, and 1 CaCl<sub>2</sub> (pH 7.2). K<sup>+</sup> currents were evoked during 1-s voltage step in 10 mV increments between  $-80$  mV and  $+60$  mV, followed by a return to  $-30$  mV for 0.5 s from a holding potential of  $-75$  mV. Recordings were performed at room temperature using an IX50 inverted microscope equipped with an FHD chamber from IonOptix (Olympus), a Multiclamp 700A Amplifier, a Digidata 1300 Analog/Digital converter and PC with pClamp9 software (Molecular Devices, Sunnyvale, CA, USA).

TABLE 1. Transcripts with  $\geq 1.5$ -fold up-regulation in female *Kcne3*<sup>-/-</sup> mouse gastrocnemius vs. *Kcne3*<sup>+/+</sup>

Gene	Fold change	P	F	Protein name	Category
<i>Musclin</i>	2.21	0.03	6.0	Musclin	Fatty acid, glucose metabolism, and other metabolic enzymes
<i>Amy1</i>	1.98	0.04	10.4	$\alpha$ -Amylase	
<i>Angptl4</i>	1.74	0.04	5.9	Angiotensin-like 4	
<i>Aldh1a1</i>	1.64	0.01	5.4	Aldehyde dehydrogenase 1 A1	
<i>Plin5</i>	1.52	0.04	6.7	Perilipin 5	
<i>Pla2g5</i>	1.52	0.046	5.6	Gp. V phospholipase A2	
<i>Lrrc52</i>	1.78	0.045	5.4	Leucine-rich repeat-cont 52	Ion channel ancillary subunits
<i>Neto2</i>	1.58	0.01	9.4	Neuropilin and tolloid-like 2	
<i>Eda2r</i>	1.79	0.03	6.2	Ectodysplasin A2 receptor	Muscle homeostasis
<i>Tagln</i>	1.52	0.03	6.7	Transgelin	Contractile protein
<i>Odf3l2</i>	2.10	0.049	5.2	Outer dense fiber of sperm tails3-like 2	Centrosome
<i>Stmn2</i>	1.57	0.01	9.6	Stathmin 2	Microtubule dynamics
<i>Mpa2l</i>	1.60	0.049	5.2	Macrophage activation 2-like	Immune response
<i>Zmynd17</i>	1.68	0.02	8.0	Zinc finger, MYND-containing 17	Unknown
<i>Gm16519</i>	1.56	0.02	8.5	Predicted gene	

Transcripts are sorted by functional category and fold change. Prefiltered to remove low-intensity signals (<5.0 in both genotypes).

## RESULTS

We previously detected KCNE3 protein in rat sartorius muscle and in the C2C12 mouse thigh muscle myoblast cell line using an in-house anti-KCNE3 antibody generated by injection of full-length recombinant mouse KCNE3 protein into rabbits (3). Since then, a different group failed

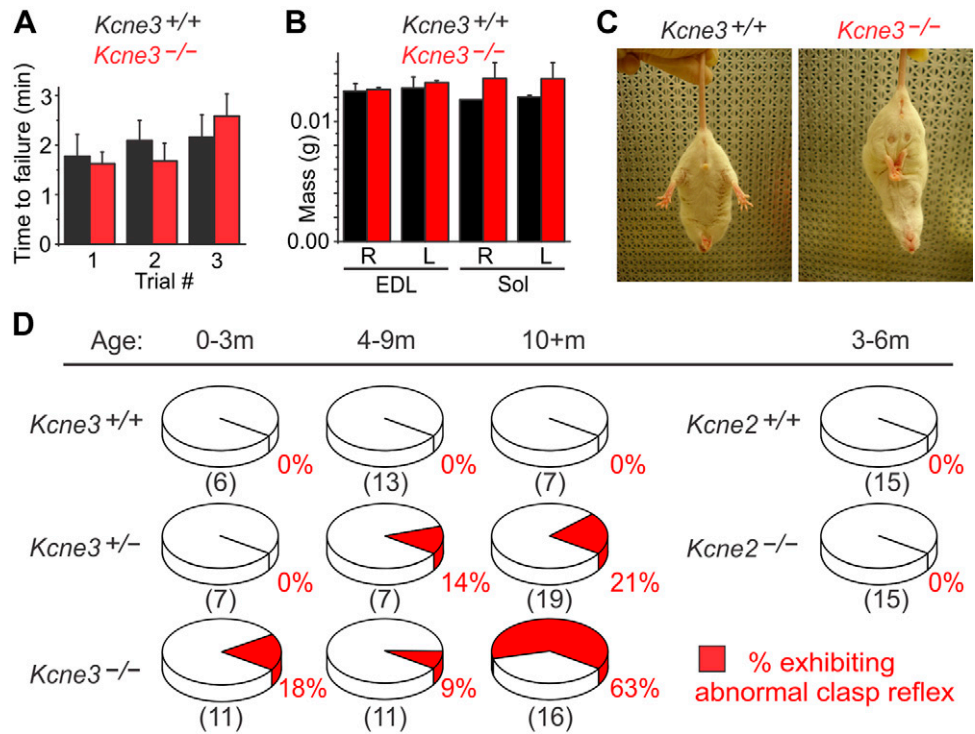
to detect KCNE3 protein in 129/SvJ-C57BL/6 mouse skeletal muscle (6). We therefore revisited this issue here. We first independently generated a *Kcne3*<sup>-/-</sup> C2J (aka B6-albino) mouse line, thereby providing a specific negative control for KCNE3 detection in skeletal muscle (Fig. 1A). Next, qPCR revealed expression of *Kcne3* transcript in skeletal muscle from *Kcne3*<sup>+/+</sup> mice but not their *Kcne3*<sup>-/-</sup>

TABLE 2. Transcripts with  $\geq 1.5$ -fold down-regulation in female *Kcne3*<sup>-/-</sup> mouse gastrocnemius vs. *Kcne3*<sup>+/+</sup>

Gene	Fold change	P	F	Protein name	Category
<i>DB</i>	-1.71	0.0003	31.4	Albumin D-box binding protein	Circadian rhythm/epigenetics
<i>Per1</i>	-1.61	0.049	5.2	Period homolog 1	
<i>Cecr2</i>	-1.55	0.049	5.2	Cat's eye syndrome chromosome regulator 2	
<i>Actc1</i>	-1.78	0.005	13.6	Actin, $\alpha$ cardiac muscle 1	Contractile protein
<i>Col1a2</i>	-1.75	0.02	9.1	$\alpha$ 2(1) collagen	Collagen and extracellular matrix-related
<i>Fn1</i>	-1.69	0.01	10.5	Fibronectin 1	
<i>Olfml3</i>	-1.62	0.04	5.5	Olfactomedin family 3	
<i>Col6a1</i>	-1.55	0.006	12.9	$\alpha$ 1(6) collagen	
<i>Lox</i>	-1.52	0.01	10.1	Lysyl oxidase	
<i>Serpinf1</i>	-1.50	0.04	6.0	Pigment epithelium-derived factor	
<i>Col3a1</i>	-1.50	0.009	11.2	$\alpha$ 1(3) collagen	
<i>Ctgf</i>	-1.82	0.009	10.7	Connective tissue growth factor	
<i>Igf1bp5</i>	-1.57	0.048	5.2	Insulin-like growth factor BP5	Growth factor related
<i>Erff1</i>	-1.52	0.02	8.4	ERBB receptor feedback inhibitor	
<i>Igf2</i>	-1.52	0.046	5.3	Insulin-like growth factor 2	
<i>Fmod</i>	-2.07	0.049	5.2	Fibromodulin	
<i>Chad</i>	-1.92	0.02	7.6	Chondroadherin	Proteoglycans, peptidases
<i>Ky</i>	-1.66	0.03	6.2	Kyphoscoliosis peptidase	
<i>Mmp2</i>	-1.50	0.02	7.6	Matrix metalloproteinase 2	
<i>Scd2</i>	-1.83	0.02	7.9	Stearoyl-coA desaturase	Fatty acid metabolism
<i>Apold1</i>	-1.60	0.04	5.5	Apolipoprotein L domain cont. 1	
<i>Sparc</i>	-1.57	0.048	5.2	Secreted protein acid, rich in Cys	Muscle damage/stress response
<i>Pxdn</i>	-1.50	0.02	8.1	Peroxidasin homolog	
<i>Mir181b-2</i>	-1.57	0.02	9.5	miRNA 181b-2	miRNA increased in endurance exercise
<i>A930039A15</i>	-2.25	0.0002	37.3	Predicted gene	Unknown
<i>Plac9</i>	-1.51	0.003	15.6	Placenta-specific 9	Unknown

Transcripts are sorted by functional category and fold change. Prefiltered to remove low-intensity signals (<5.0 in both genotypes).

**Figure 3.** *Kcne3*<sup>-/-</sup> mice exhibit abnormal clasp behavior. **A)** Mean time to failure on rotarod for 6-mo-old *Kcne3*<sup>+/+</sup> and *Kcne3*<sup>-/-</sup> mice (*n* = 10 per genotype); no significant difference between genotypes (*P* > 0.05). **B)** Mean mass for right (R) and left (L) EDL and soleus (Sol) muscles from *Kcne3*<sup>+/+</sup> and *Kcne3*<sup>-/-</sup> mice (*n* = 3–5); no significant difference between genotypes (*P* > 0.05). **C)** Exemplar normal wild-type mouse behavior versus abnormal hind-limb clasp reflex in *Kcne3*<sup>-/-</sup> mouse upon tail suspension. **D)** Percentage of mice exhibiting abnormal hind-limb clasp reflex upon tail suspension for genotypes and age groups as indicated. Sample sizes are provided in parentheses below each group.



littermates (Fig. 1B). Similarly, Western blot analysis with a commercially available antibody (Alomone Labs) raised to a human KCNE3 C-terminal epitope indicated robust expression of KCNE3 protein in gastrocnemius, soleus, and extensor digitorum longus (EDL) muscle from *Kcne3*<sup>+/+</sup> mice, but not in the equivalent tissues from *Kcne3*<sup>-/-</sup> mice. As we previously observed (3), here the predicted bi- and triglycosylated forms of KCNE3 predominated, but a lower weight form at 15 kDa was also visible in muscle from *Kcne3*<sup>+/-</sup> mice (Fig. 1C).

Having established that KCNE3 is expressed in mouse skeletal muscle, we performed whole-transcript genome expression analysis to determine the effects of *Kcne3* deletion on skeletal muscle tissue gene expression using the GeneAtlas microarray system (Affymetrix), which uses an average of 26 probes per gene to yield an accurate, quantitative, and highly reproducible picture of shifts in the transcriptome. Principal component analysis (11) indicated close grouping of gastrocnemius transcriptomes in the group of *Kcne3*<sup>+/+</sup> mice, whereas *Kcne3*<sup>-/-</sup> mouse gastrocnemius transcriptomes exhibited much more scatter between individuals, suggesting *Kcne3* deletion caused aberrant development or other pathophysiological processes in skeletal muscle (Fig. 2A).

Using this unbiased (noncandidate) approach, we detected 26 skeletal muscle transcripts that were up-regulated (Table 1) and 15 that were down-regulated (Table 2), by at least 1.5-fold (*P* < 0.05), by *Kcne3* deletion (*n* = 5–6 mice per genotype). Up-regulation of *musclin*, which is only produced by fast-twitch fibers (21), and transcripts for genes involved in oxidative/fatty acid metabolism (*Angptl4*, *Pla2g5*, *perilipin*, and *aldehyde dehydrogenase*) suggested a fiber-type switch favoring fast, oxidative fibers. This was supported by histochemical

data indicating a lack of overt pathology with hematoxylin and eosin staining (Fig. 2B) but an increase in fibers positive for succinate dehydrogenase (Fig. 2C) and an increase in the relative amount of myosin heavy chain type IIa positive (fast oxidative) fibers (*n* = 3 mice, 4–5 sections per genotype, *P* = 0.015) (Fig. 2D, E). This switch was reminiscent of the Met1592Val Nav1.4 knock-in mouse model of human myotonia (17). Also notable were increases in transcript expression for ion channel ancillary subunits *Lrrc52* and *Neto2*, *transgelin* (a contractile protein the expression of which is increased by electrical stimulation), and *Eda2r* (ectodysplasin A2 receptor), a marker of myodegeneration (Table 1).

The down-regulated transcript group was dominated by genes involved in extracellular matrix formation, including collagen (*Col1A2*, *Col1A3*, and *Col6A1*), *Lox* (lysyl oxidase, which cross-links collagen), and growth factors *Ctgf*, *Errf1*, *Igf1*, and *Igf2*. Also down-regulated were several genes whose dysfunction or loss is linked to myotonic dystrophy, atrophy, or muscle weakness (*fibronectin 1*, *connective tissue growth factor*, *Sparc*, *Mmp2*, *Fmod*, and the aforementioned collagens), and metabolism-related proteins either linked to circadian control (*Dbp* and *Per1*) or fatty acid metabolism (*Scd2* and *Apold1*) (Table 2).

Overall, the data suggested remodeling of skeletal muscle composition in *Kcne3*<sup>-/-</sup> mice. Because KCNE3 is a K<sup>v</sup> channel ancillary subunit, we also took a more targeted approach to transcript analysis of *Kcne3*<sup>-/-</sup> skeletal muscle tissue, searching for all the K<sup>+</sup> channel transcripts present in the microarray probe set and tabulating their expression. Out of a total of 69 K<sup>+</sup> channel  $\alpha$  subunit transcripts annotated, the skeletal muscle expression levels of only 3 were altered by *Kcne3* deletion (as indicated



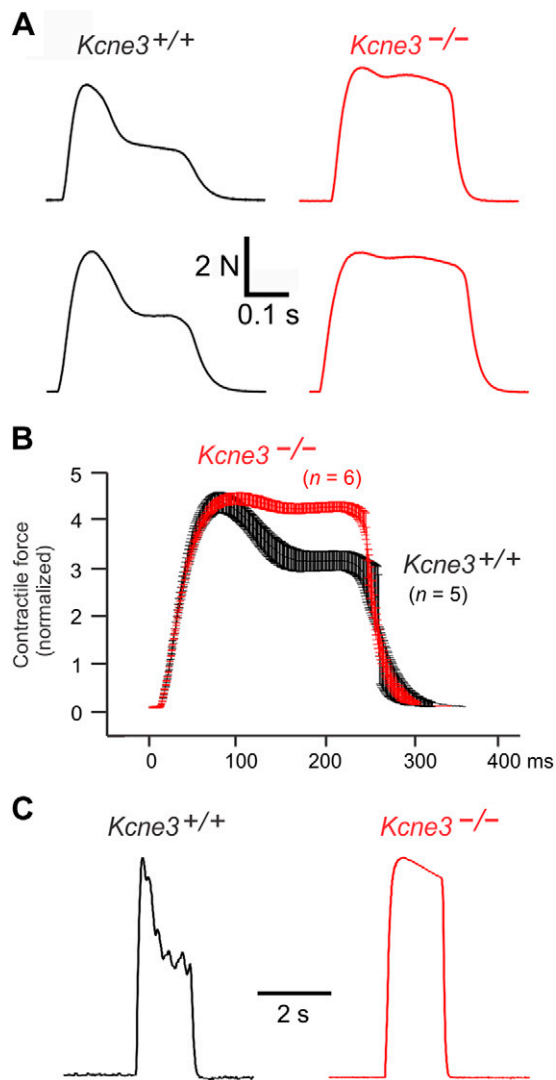


**Figure 4.** *Kcne3*<sup>-/-</sup> mouse skeletal muscle exhibits abnormally sustained contraction. **A)** *In vivo* hind-limb muscle contractility. Representative maximal force tracings from *Kcne3*<sup>+/+</sup> (left) and *Kcne3*<sup>-/-</sup> (right) mice from *in vivo* measurement of contractility of hind-limb muscle group using custom *in vivo* contractile apparatus. **B)** Pooled data of maximal force tracings from *Kcne3*<sup>+/+</sup> (black, *n* = 5 animals) and *Kcne3*<sup>-/-</sup> (red, *n* = 6 animals) mice from *in vivo* measurement of contractility of hind-limb muscle group as in **A**. **C)** *In vitro* EDL contractility. Representative maximal force tracings from *Kcne3*<sup>+/+</sup> (left, black) and *Kcne3*<sup>-/-</sup> (right, red) mice from *in vitro* measurement of contractility of hind-limb muscle group. Traces are representative of 2 muscles each from 4 different mice of each genotype.

by  $P < 0.05$ ). Strikingly, 2 of these 3 are known partners of KCNE3. Thus, *Kcnc4*, which encodes  $K_{v3.4}$ , and *Kcnh2*, which encodes the mouse *ether-a-go-go related gene* (mERG), were both down-regulated; the other was the 2-pore-domain  $K^+$  leak channel TRAAK, *Kcnk4*, which was up-regulated (Supplemental Table 1). *Kcnc4* transcript down-regulation was specific even within the *Kcnc* sub-family (Fig. 2F) and was confirmed at the protein level by Western blot analysis (Fig. 2G, H).

We next examined the effects of *Kcne3* gene deletion on skeletal muscle function. In agreement with a previous

report (6), rotarod performance was not impaired by *Kcne3* deletion (Fig. 3A); nor was muscle mass altered (Fig. 3B). Turning to functional assays not reportedly used in prior studies of *Kcne3*<sup>-/-</sup> mouse muscle pathology, we found that upon tail suspension, 10 (63%) of 16 *Kcne3*<sup>-/-</sup> mice and 4 (21%) of 19 *Kcne3*<sup>+/-</sup> mice aged 10 mo and older exhibited abnormal hind-limb clasping behavior (Fig. 3C, D) similar to what is observed in myotonia (17). Younger *Kcne3*<sup>-/-</sup> and *Kcne3*<sup>+/-</sup> mice exhibited similar behavior but with lower penetrance (Fig. 3D). In contrast, hind-limb clasping behavior was not observed at any age in *Kcne3*<sup>+/+</sup> littermates (*n* = 26); nor did it occur in C57BL/6 *Kcne2*<sup>+/+</sup> (*n* = 15) or *Kcne2*<sup>-/-</sup> mice (*n* = 15) utilized as a control for other *Kcne* gene disruption (Fig. 3D). The findings suggest a specific, *Kcne3* gene-dependent form of muscle abnormality.

*In vivo* skeletal muscle contractility assays, also to our knowledge not previously utilized to quantify *Kcne3*<sup>-/-</sup> muscle function, revealed loss of the typical biphasic decline in contractile force with repetitive stimuli of hind-limb muscle of *Kcne3*<sup>-/-</sup> mice compared to age-matched *Kcne3*<sup>+/+</sup> littermates (Fig. 4A). This delayed relaxation was observed consistently in preparations from multiple mice (Fig. 4B). Typically, the hind-limb muscle group in mice displays this biphasic contractile profile because the gastrocnemius contains abundant fast-twitch type II muscle fibers (22).

It is likely that the fiber type switching found in *Kcne3*<sup>-/-</sup> mouse skeletal muscle (Table 1 and Fig. 2) results in a prolonged maintenance of contractile force after repetitive stimulation. To test the hypothesis that this defect arose primarily from the skeletal muscle itself rather than loss of KCNE3 function in, for example, the nervous system, analogous experiments were performed with *ex vivo* EDL muscles *in vitro* (Fig. 4C). These studies showed similar changes in force output as in the *in vivo* analysis, thus supporting the observations from *in vivo* contractility analyses.

Transcriptomic analysis indicated no significant changes in expression of *Acta1*, *Cacna1s*, *Calsequestrin 2*, *Ryr1*, *Sarcalumenin*, *Serca1*, or *Serca2* (Fig. 5A), verified by Western blot analysis (Fig. 5B, C); there did appear to be a reduction in expression of *Calsequestrin 1* transcript, but this was not accompanied by a reduction in protein expression (Fig. 5B, C). However, the lack of overt expression remodeling does not rule out changes in posttranslational modification or function of these proteins involved in  $Ca^{2+}$  regulation of muscle contraction.

Finally, we isolated, cultured, and patch-clamped myoblasts from the gastrocnemius muscle of >1-yr-old *Kcne3*<sup>+/+</sup> and *Kcne3*<sup>-/-</sup> mice. We detected a fast-inactivating outward current in *Kcne3*<sup>+/+</sup> myoblasts, which displayed a similar inactivation rate to that reported for native KCNC4 in dorsal root ganglion neurons (23) (Fig. 6A). *Kcne3* deletion did not alter mean peak current in isolated myoblasts, but sustained current (recorded at the end of 1-s pulses) tended to be lower in myoblasts isolated from *Kcne3*<sup>-/-</sup> mice compared to wild type (Fig. 6A–C). In addition, both the fast and slow components of the transient outward current in myoblasts from *Kcne3*<sup>-/-</sup> mice ( $0.51 \pm 0.08$  and  $2.80 \pm 0.31$  ms, respectively) exhibited



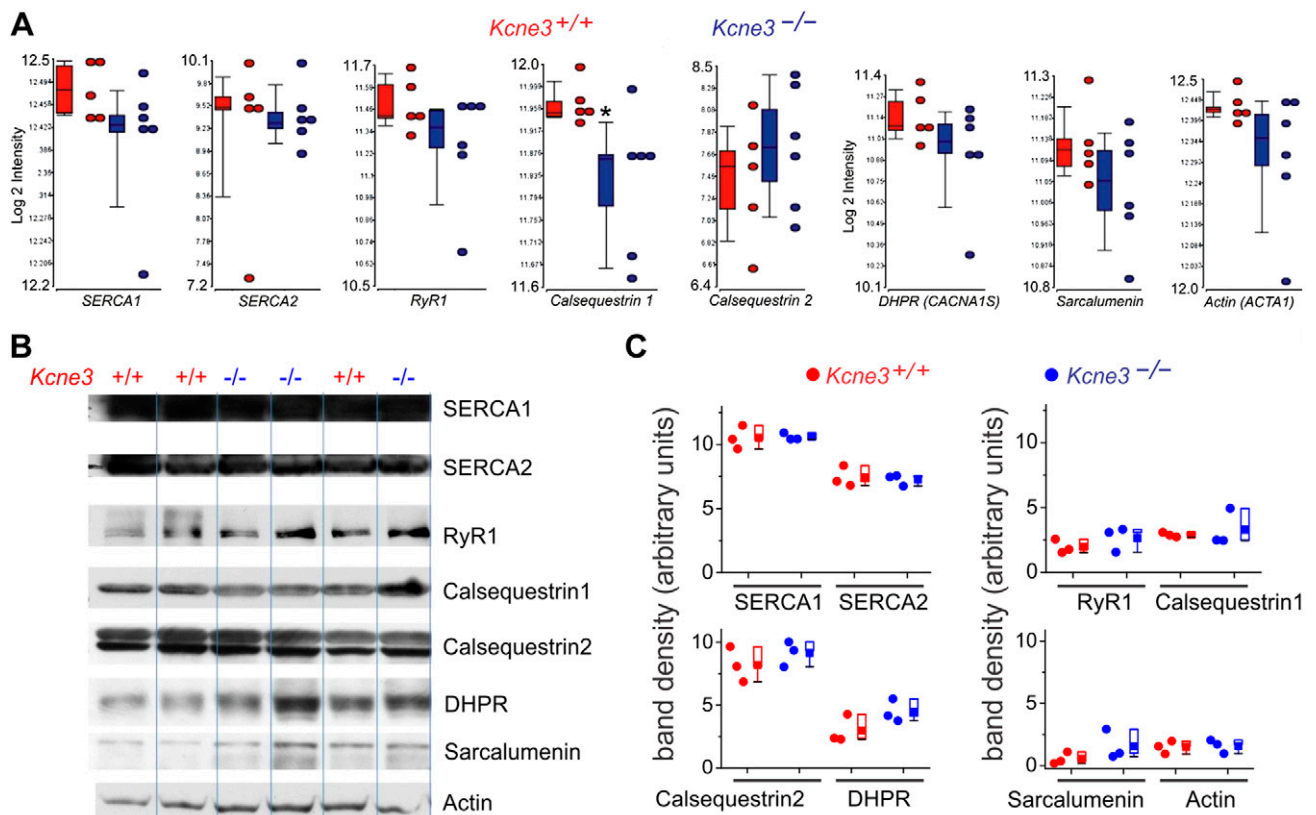


**Figure 5.** Skeletal muscle excitation–contraction coupling transcript and protein expression in *Kcne3*<sup>+/+</sup> and *Kcne3*<sup>-/-</sup> mice. **A**) Log<sub>2</sub> intensity of transcript expression in gastrocnemius muscle extracts from *Kcne3*<sup>+/+</sup> (*n* = 5) and *Kcne3*<sup>-/-</sup> (*n* = 6) mice for various muscle excitation–contraction coupling proteins. \**P* < 0.05 between genotypes. **B**) Western blots of gastrocnemius muscle extracts from *Kcne3*<sup>+/+</sup> and *Kcne3*<sup>-/-</sup> (*n* = 3) mice for various muscle excitation–contraction coupling proteins. **C**) Relative band densities quantified from blots in **B**. None of the expression levels between genotypes achieved statistical significance. *P* > 0.05.

faster mean decay compared to wild type ( $0.744 \pm 0.16$  ms and  $8.98 \pm 3.53$  ms, respectively) (*n* = 8–22; *P* = 0.009 and *P* = 0.16, respectively). The relative amplitude of the slow component was greater in myoblasts from *Kcne3*<sup>-/-</sup> ( $0.30 \pm 0.06$ ) vs. *Kcne3*<sup>+/+</sup> ( $0.18 \pm 0.06$ ) mice (*n* = 8–22; *P* = 0.23) (Fig. 6D–F). Additionally, the sum of the amplitudes of the fast and slow components of the transient current (an estimate of the amplitude of the total transient current) was marginally lower in myoblasts from *Kcne3*<sup>-/-</sup> (slow, fast, total =  $74 \pm 14$ ,  $238 \pm 53$ ,  $312 \pm 52$  pA) versus *Kcne3*<sup>+/+</sup> (slow, fast, total =  $39 \pm 10$ ,  $319 \pm 112$ ,  $358 \pm 112$  pA) mice, although this did not reach statistical significance (*n* = 8–22; *P* > 0.05).

## DISCUSSION

*KCNE3* coassembles with *KCNC4* (*K<sub>v</sub>3.4*) and left-shifts the voltage dependence of its activation by ~45 mV, converting *KCNC4* to a subthreshold-activating *K<sub>v</sub>* channel that can contribute to skeletal muscle resting membrane potential. An R83H mutation in human *KCNE3* was previously found to associate with periodic paralysis and rendered *KCNC4*-*KCNE3* channels sensitive to proton inhibition at higher pH than wild-type channels (3, 24). The nondystrophic myotonias and periodic paralyses

comprise a group of debilitating disorders stemming from abnormal electrical activity in skeletal muscle and are characterized by abnormal muscle relaxation (myotonia), weakness, or both. Most human cases have been linked to mutations in *CLCN1*, which encodes a skeletal muscle voltage-gated chloride channel (25), or in *SCN4A*, which encodes a skeletal muscle voltage-gated sodium channel (26, 27), but several forms have been linked to mutations in genes that encode *K<sup>+</sup>* channel subunits (28, 29), the first of which was *KCNE3* (3).

While others have since questioned this association (4, 5), we contend the current data provide supporting evidence of the importance of *KCNE3* in skeletal muscle physiology. The previous negative study of *KCNE3* expression and functional relevance in mouse skeletal muscle was performed on mixed 129/SvJ-C57BL/6 mice (6), whereas our current study utilized C2J mice. It is possible that *KCNE3* expression in mice is strain dependent; alternatively, the differing genetic backgrounds of the 2 lines may simply alter the susceptibility of skeletal muscle function to *Kcne3* deletion. With respect to differing conclusions from different human genetics studies of an association between R83H-*KCNE3* and periodic paralysis, our current data in mice suggest this may be worth reexamining. While we did not observe periodic paralysis in *Kcne3*<sup>-/-</sup> mice, we observed contractile abnormalities,

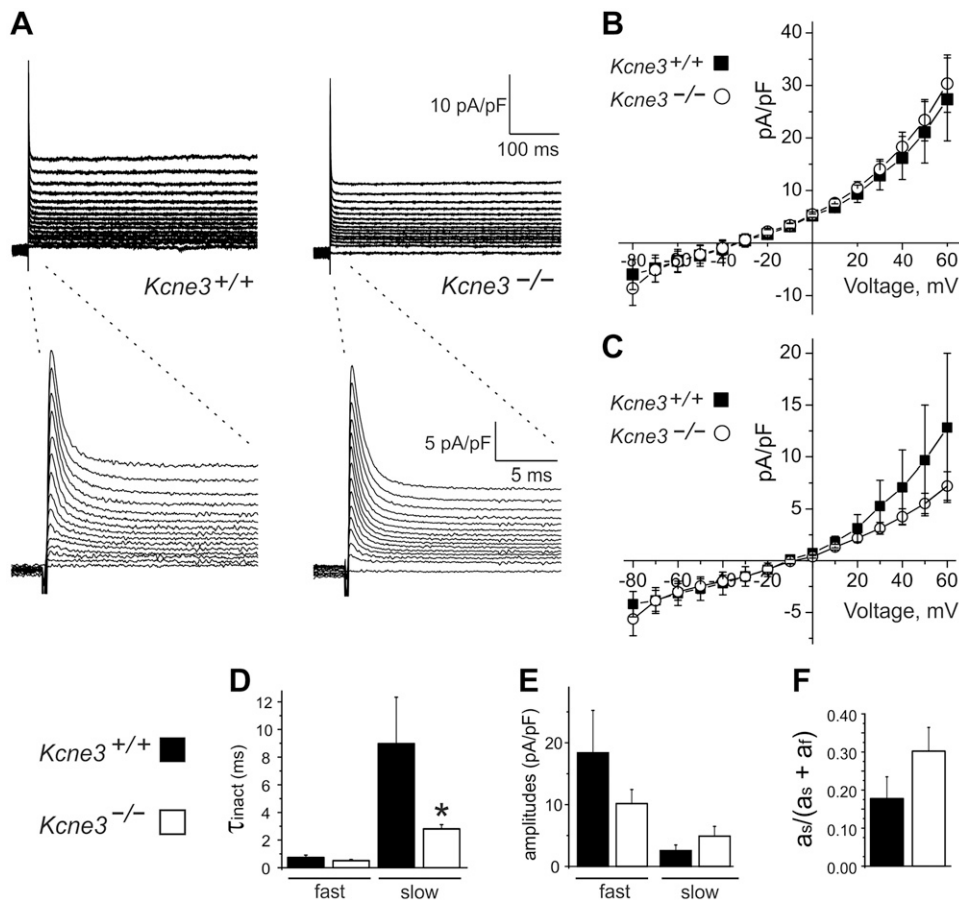


**Figure 6.** *Kcne3* deletion alters skeletal myoblast outward currents. **A)** Averaged traces recorded from myoblasts in whole-cell patch-clamp configuration during 1-s pulses between  $-80$  mV and  $+60$  mV from holding potential of  $-75$  mV;  $n = 8$ –22 cells (from 3 myoblast preparations per genotype; each preparation was pooled from skeletal muscle from 3 mice per genotype, total of 9 mice per genotype used). Lower traces show expanded view during first 20 ms of test pulse. **B)** Mean peak outward current density *vs.* voltage measured from myoblast traces as in **A**;  $n = 8$ –22 cells. Error bars indicate SEM. **C)** Mean sustained (at 1 s) outward current density *vs.* voltage measured from myoblast traces as in **B**. **D)** Mean  $\tau$  of inactivation for fast and slow components of current decay after fitting with double exponential function, for cells as in **B** ( $n = 8$ –22 per genotype). \* $P < 0.05$  *vs.*  $Kcne3^{+/+}$ . **E)** Mean amplitudes (expressed as current density) for fast and slow components of decay after fitting with double exponential function for cells as in **B** ( $n = 8$ –22 per genotype). **F)** Mean relative amplitude of slow component of inactivation after fitting with double exponential function for cells as in **B** ( $n = 8$ –22 per genotype).

in **B** ( $n = 8$ –22 per genotype). **F)** Mean relative amplitude of slow component of inactivation after fitting with double exponential function for cells as in **B** ( $n = 8$ –22 per genotype).

transcriptome remodeling (most strikingly of KCNC4, which we originally discovered to be a skeletal muscle partner of KCNE3 (3)), as well as evidence of fiber-type switching, consistent with a role for KCNE3 in skeletal muscle function, and/or a direct or indirect effect on skeletal muscle function of *Kcne3* deletion.

In addition, we observed decreased sustained outward current and faster decay of the transient outward current in patch-clamped myoblasts isolated from *Kcne3*<sup>-/-</sup> mice compared to those from *Kcne3*<sup>+/+</sup> mice (Fig. 6). We previously also found that KCNE3 coexpression increased activity of the KCNC4 potassium channel (3, 24), and here we found that *Kcne3* deletion reduced *Kcnc4* transcript and protein expression in mouse skeletal muscle (Fig. 2). Taken together, these findings suggest that *Kcne3* deletion reduces KCNC4 activity in skeletal myocytes. This provides a possible mechanistic explanation for the increase in sustained contractility we observed in *Kcne3*<sup>-/-</sup> hind limbs (Fig. 4), as decreased repolarizing outward K<sup>+</sup> current would be predicted to make the tissue hyperexcitable, analogous to loss of function in the CLCN1 chloride channel, which prolongs contraction and causes myotonia (30). Despite the lack of observed CLCN1 transcript remodeling, it is also feasible that CLCN1 current was indirectly altered by *Kcne3* deletion, but we did not resolve that here. KCNC4 transcript expression was previously found to be reduced in skeletal muscle from a myotonic mouse mutant (ADR\*2J) (31). Our findings here—that

KCNC4 transcript and protein expression are reduced in a mouse with prolonged contraction—are consistent with those data. KCNC4 expression was also previously found to be reduced in denervated muscle compared to innervated (31); it is important to note, therefore, that our myoblast recordings may not fully reflect changes in KCNC4 current properties in native active muscle resulting from *Kcne3* deletion, and future work to examine the cellular electrophysiologic effects of *Kcne3* deletion in innervated muscle fibers may resolve further differences.

With respect to the other 2 channel transcripts we found to be altered in *Kcne3*<sup>-/-</sup> skeletal muscle, KCNE3 inhibits human KCNH2 when coexpressed in oocytes or immortal cell lines. *Kcne3* deletion would be expected therefore to increase KCNH2 current, but it is not known whether KCNE3 regulation of KCNH2 occurs in skeletal muscle (or indeed anywhere *in vivo*). KCNH2 is up-regulated in atrophic muscle and its inhibition reduced muscular atrophy in a mouse model (32), but the role of KCNH2 in normal mouse skeletal muscle is not known. KCNC4 was previously detected in mouse skeletal muscle and was found to be up-regulated during differentiation from myoblasts to myotubes *in vitro* (33), but its role in skeletal muscle is not known, and none of the KCNK (K2P) channels has been yet discovered to be regulated by KCNE proteins. Interestingly, *Kcnc1* (K<sub>v</sub>3.1) deletion was previously found to result in abnormally sustained contraction in mouse skeletal muscle (34). While KCNC1

transcript expression was not altered in *Kcne3*<sup>-/-</sup> mouse skeletal muscle (Fig. 2), the delayed rectifier potassium channel KCNC1 is regulated by KCNE3 *in vitro* (35), and it is therefore another possible partner for KCNE3 in skeletal muscle.

Despite our findings in mice, it is possible that KCNE3 plays a relatively minor role in human skeletal muscle and that human KCNE3-associated skeletal muscle dysfunction is rare, of low penetrance, requires modifier genes, or is indeed coincidental (*e.g.*, if KCNE3 disruption affects skeletal muscle function in mice but not human beings). Alternatively, KCNE3 might only be present in select cells or regions of skeletal muscle, but important in specific cell populations. We and others recently showed that despite *Kcne3* being undetectable in mouse cardiac muscle (atria or ventricles), targeted *Kcne3* deletion can predispose to ventricular and atrial cardiac arrhythmias in mice. The underlying mechanism is that *Kcne3* deletion triggers an autoimmune response in the adrenal glands, which is associated with hyperaldosteronism; this in turn promotes arrhythmogenesis. This trait was observed independently in 2 different *Kcne3*<sup>-/-</sup> mouse lines of different strains (36, 37). It is therefore possible that human KCNE3-associated cardiac arrhythmias and/or skeletal muscle dysfunction also require elevated aldosterone and that this only manifests in select individuals. KCNE3 has been detected by us and other groups in human heart, and human KCNE3 sequence variants are associated with the cardiac arrhythmias atrial fibrillation and Brugada syndrome (38–43). It is not known whether autoimmune-associated hyperaldosteronism plays a role in human KCNE3-linked arrhythmogenesis.

Finally, it is worth noting that we recently discovered a longer form of KCNE3 (KCNE3L), extended by a previously undetected exon 1-encoded N-terminal fragment. This extends the protein by 44 residues and alters its effects on some K<sub>v</sub> channel  $\alpha$  subunit partners. However, KCNE3L has only been observed thus far in primate genomes, and it appears to be absent in mice because in the mouse genome the *Kcne3* gene lacks the ATG start site on exon 1 (38). The role of KCNE3 in human and mouse tissues, including in skeletal muscle, could be different as a result of this major sequence difference, in addition to any other mismatches in tissue expression and other physiologic divergences between the 2 species. Further analyses of the skeletal muscle defect in *Kcne3*<sup>-/-</sup> C2J mice will be targeted toward elucidation of its precise molecular and electrical etiology, with the goal of directing future investigations of the putative role of KCNE3 in human skeletal muscle function and disease, albeit with the caveats described above. FJ

## ACKNOWLEDGMENTS

This work was supported by the U.S. National Institutes of Health (NIH) National Heart, Lung, and Blood Institute (NHLBI) (Grant R01 HL079275 to G.W.A.), and University of California, Irvine setup funds (to G.W.A.). N.W. was supported by the NIH National Institute of Arthritis and Musculoskeletal and Skin Diseases (Grant R01 AR063084). X.Z. is grateful for support from NIH NHLBI Grant R01 HL116826. The authors

thank R. Kant and C. Cao (University of California, Irvine) for technical support.

## AUTHOR CONTRIBUTIONS

N. Weisleder and G. W. Abbott designed research; E. C. King, V. Patel, M. Anand, X. Zhao, S. M. Crump, Z. Hu, and G. W. Abbott performed research; G. W. Abbott wrote the article; and all authors analyzed the data and edited the article.

## REFERENCES

1. Abbott, G. W., Sesti, F., Splawski, I., Buck, M. E., Lehmann, M. H., Timothy, K. W., Keating, M. T., and Goldstein, S. A. (1999) MiRP1 forms IKr potassium channels with HERG and is associated with cardiac arrhythmia. *Cell* **97**, 175–187
2. Schroeder, B. C., Waldegger, S., Fehr, S., Bleich, M., Warth, R., Greger, R., and Jentsch, T. J. (2000) A constitutively open potassium channel formed by KCNQ1 and KCNE3. *Nature* **403**, 196–199
3. Abbott, G. W., Butler, M. H., Bendahhou, S., Dalakas, M. C., Ptacek, L. J., and Goldstein, S. A. (2001) MiRP2 forms potassium channels in skeletal muscle with K<sub>v</sub>3.4 and is associated with periodic paralysis. *Cell* **104**, 217–231
4. Sternberg, D., Tabti, N., Fournier, E., Hainque, B., and Fontaine, B. (2003) Lack of association of the potassium channel-associated peptide MiRP2-R83H variant with periodic paralysis. *Neurology* **61**, 857–859
5. Jurkat-Rott, K., and Lehmann-Horn, F. (2004) Periodic paralysis mutation MiRP2-R83H in controls: interpretations and general recommendation. *Neurology* **62**, 1012–1015
6. Preston, P., Wartosch, L., Günzel, D., Fromm, M., Kongsuphol, P., Ousingsawat, J., Kunzelmann, K., Barhanin, J., Warth, R., and Jentsch, T. J. (2010) Disruption of the K<sup>+</sup> channel beta-subunit KCNE3 reveals an important role in intestinal and tracheal Cl<sup>-</sup> transport. *J. Biol. Chem.* **285**, 7165–7175
7. Roepke, T. K., King, E. C., Purtell, K., Kanda, V. A., Lerner, D. J., and Abbott, G. W. (2011) Genetic dissection reveals unexpected influence of beta subunits on KCNQ1 K<sup>+</sup> channel polarized trafficking *in vivo*. *FASEB J.* **25**, 727–736
8. Weisleder, N., Ferrante, C., Hirata, Y., Collet, C., Chu, Y., Cheng, H., Takeshima, H., and Ma, J. (2007) Systemic ablation of RyR3 alters Ca<sup>2+</sup> spark signaling in adult skeletal muscle. *Cell Calcium* **42**, 548–555
9. Zhao, X., Min, C. K., Ko, J. K., Parness, J., Kim, D. H., Weisleder, N., and Ma, J. (2010) Increased store-operated Ca<sup>2+</sup> entry in skeletal muscle with reduced calsequestrin-1 expression. *Biophys. J.* **99**, 1556–1564
10. Bolstad, B. M., Irizarry, R. A., Astrand, M., and Speed, T. P. (2003) A comparison of normalization methods for high density oligonucleotide array data based on variance and bias. *Bioinformatics* **19**, 185–193
11. Jolliffe, I. T. (1986) *Principal Component Analysis*, Springer-Verlag, New York
12. Eisenhart, C. (1947) The assumptions underlying the analysis of variance. *Biometrics* **3**, 1–21
13. Tamhane, A. C., and Dunlop, D. D. (2006) *Statistics and Data Analysis from Elementary to Intermediate*, Prentice-Hall, Upper Saddle River, NJ, USA
14. Benjamini, Y., and Hochberg, Y. (1995) Controlling the false discovery rate: a practical and powerful approach to multiple testing. *JRSS B* **57**, 289–300
15. Muller, K. E., and Peterson, B. L. (1984) Practical methods for computing power in testing the multivariate general linear hypothesis. *Comput. Stat. Data Anal.* **2**, 143–158
16. Lee, C. S., Dagnino-Acosta, A., Yarotsky, V., Hanna, A., Lyfenko, A., Knoblauch, M., Georgiou, D. K., Poche, R. A., Swank, M. W., Long, C., Ismailov, I., Lanner, J., Tran, T., Dong, K., Rodney, G. G., Dickinson, M. E., Beeton, C., Zhang, P., Dirksen, R. T., and Hamilton, S. L. (2015) Ca(2+) permeation and/or binding to Cav1.1 fine-tunes skeletal muscle Ca(2+) signaling to sustain muscle function. *Skelet. Muscle* **5**, 4
17. Hayward, L. J., Kim, J. S., Lee, M. Y., Zhou, H., Kim, J. W., Misra, K., Salajegheh, M., Wu, F. F., Matsuda, C., Reid, V., Cros, D., Hoffman, E. P., Renaud, J. M., Cannon, S. C., and Brown, R. H., Jr. (2008)



- Targeted mutation of mouse skeletal muscle sodium channel produces myotonia and potassium-sensitive weakness. *J. Clin. Invest.* **118**, 1437–1449
18. Weber, H., Rauch, A., Adamski, S., Chakravarthy, K., Kulkarni, A., Dogdas, B., Bendtsen, C., Kath, G., Alves, S. E., Wilkinson, H. A., and Chiu, C. S. (2012) Automated rodent in situ muscle contraction assay and myofiber organization analysis in sarcopenia animal models. *J. Appl. Physiol.* **112**, 2087–2098
  19. Weisleder, N., Brotto, M., Komazaki, S., Pan, Z., Zhao, X., Nosek, T., Parness, J., Takeshima, H., and Ma, J. (2006) Muscle aging is associated with compromised  $Ca^{2+}$  spark signaling and segregated intracellular  $Ca^{2+}$  release. *J. Cell Biol.* **174**, 639–645
  20. Mille, M., Koenig, X., Zebedin, E., Uhrin, P., Cervenka, R., Todt, H., and Hilber, K. (2009) Sodium current properties of primary skeletal myocytes and cardiomyocytes derived from different mouse strains. *Pflugers Arch.* **457**, 1023–1033
  21. Banzet, S., Koulmann, N., Sanchez, H., Serrurier, B., Peinnequin, A., and Bigard, A. X. (2007) Myosin gene expression is strongly related to fast-glycolytic phenotype. *Biochem. Biophys. Res. Commun.* **353**, 713–718
  22. Hayasaki, H., Shimada, M., Kanbara, K., and Watanabe, M. (2001) Regional difference in muscle fiber type and glucose uptake of mouse gastrocnemius at rest. *Cell. Mol. Biol. (Noisy-le-grand)* **47**, OL135–OL140
  23. Ritter, D. M., Zemel, B. M., Lepore, A. C., and Covarrubias, M. (2015)  $K_{v}3.4$  channel function and dysfunction in nociceptors. *Channels (Austin)* **9**, 209–217
  24. Abbott, G. W., Butler, M. H., and Goldstein, S. A. (2006) Phosphorylation and protonation of neighboring MiRP2 sites: function and pathophysiology of MiRP2- $K_{v}3.4$  potassium channels in periodic paralysis. *FASEB J.* **20**, 293–301
  25. Koch, M. C., Steinmeyer, K., Lorenz, C., Ricker, K., Wolf, F., Otto, M., Zoll, B., Lehmann-Horn, F., Grzeschik, K. H., and Jentsch, T. J. (1992) The skeletal muscle chloride channel in dominant and recessive human myotonia. *Science* **257**, 797–800
  26. Fontaine, B., Khurana, T. S., Hoffman, E. P., Bruns, G. A., Haines, J. L., Trofatter, J. A., Hanson, M. P., Rich, J., McFarlane, H., and Yasek, D. M., et al. (1990) Hyperkalemic periodic paralysis and the adult muscle sodium channel alpha-subunit gene. *Science* **250**, 1000–1002
  27. Ptáček, L. J., Trimmer, J. S., Agnew, W. S., Roberts, J. W., Petajan, J. H., and Leppert, M. (1991) Paramyotonia congenita and hyperkalemic periodic paralysis map to the same sodium-channel gene locus. *Am. J. Hum. Genet.* **49**, 851–854
  28. Plaster, N. M., Tawil, R., Tristani-Firouzi, M., Canún, S., Bendahhou, S., Tsunoda, A., Donaldson, M. R., Iannaccone, S. T., Brunt, E., Barohn, R., Clark, J., Deymeer, F., George, A. L., Jr., Fish, F. A., Hahn, A., Nitu, A., Ozdemir, C., Serdaroglu, P., Subramony, S. H., Wolfe, G., Fu, Y. H., and Ptáček, L. J. (2001) Mutations in  $Kir2.1$  cause the developmental and episodic electrical phenotypes of Andersen's syndrome. *Cell* **105**, 511–519
  29. Ryan, D. P., da Silva, M. R., Soong, T. W., Fontaine, B., Donaldson, M. R., Kung, A. W., Jongjaroenprasert, W., Liang, M. C., Khoo, D. H., Cheah, J. S., Ho, S. C., Bernstein, H. S., Maciel, R. M., Brown, R. H., Jr., and Ptáček, L. J. (2010) Mutations in potassium channel  $Kir2.6$  cause susceptibility to thyrotoxic hypokalemic periodic paralysis. *Cell* **140**, 88–98
  30. George, A. L., Jr. (1995) Molecular genetics of ion channel diseases. *Kidney Int.* **48**, 1180–1190
  31. Vullhorst, D., Klocke, R., Bartsch, J. W., and Jockusch, H. (1998) Expression of the potassium channel  $K_{v}3.4$  in mouse skeletal muscle parallels fiber type maturation and depends on excitation pattern. *FEBS Lett.* **421**, 259–262
  32. Wang, X., Hockerman, G. H., Green III, H. W., Babbs, C. F., Mohammad, S. I., Gerrard, D., Latour, M. A., London, B., Hannon, K. M., and Pond, A. L. (2006) Mergla  $K^{+}$  channel induces skeletal muscle atrophy by activating the ubiquitin proteasome pathway. *FASEB J.* **20**, 1531–1533
  33. Afzali, A. M., Ruck, T., Herrmann, A. M., Iking, J., Sommer, C., Kleinschnitz, C., Preuß, C., Stenzel, W., Budde, T., Wiendl, H., Bittner, S., and Meuth, S. G. (2016) The potassium channels TASK2 and TREK1 regulate functional differentiation of murine skeletal muscle cells. *Am. J. Physiol. Cell Physiol.* **311**, C583–C595
  34. Sánchez, J. A., Ho, C. S., Vaughan, D. M., Garcia, M. C., Grange, R. W., and Joho, R. H. (2000) Muscle and motor-skill dysfunction in a  $K^{+}$  channel-deficient mouse are not due to altered muscle excitability or fiber type but depend on the genetic background. *Pflugers Arch.* **440**, 34–41
  35. Lewis, A., McCrossan, Z. A., and Abbott, G. W. (2004) MinK, MiRP1, and MiRP2 diversify  $K_{v}3.1$  and  $K_{v}3.2$  potassium channel gating. *J. Biol. Chem.* **279**, 7884–7892
  36. Hu, Z., Crump, S. M., Anand, M., Kant, R., Levi, R., and Abbott, G. W. (2014) *Kcne3* deletion initiates extracardiac arrhythmogenesis in mice. *FASEB J.* **28**, 935–945
  37. Lisewski, U., Koehncke, C., Wilck, N., Buschmeyer, B., Pieske, B., and Roepeke, T. K. (2016) Increased aldosterone-dependent  $K_{v}1.5$  recycling predisposes to pacing-induced atrial fibrillation in *Kcne3*<sup>-/-</sup> mice. *FASEB J.* **30**, 2476–2489
  38. Abbott, G. W. (2016) Novel exon 1 protein-coding regions N-terminally extend human *KCNE3* and *KCNE4*. *FASEB J.* **30**, 2959–2969
  39. Delpón, E., Cordeiro, J. M., Núñez, L., Thomsen, P. E., Guerchicoff, A., Pollevick, G. D., Wu, Y., Kanters, J. K., Larsen, C. T., Hofman-Bang, J., Burashnikov, E., Christiansen, M., and Antzelevitch, C. (2008) Functional effects of *KCNE3* mutation and its role in the development of Brugada syndrome. *Circ. Arrhythm. Electrophysiol.* **1**, 209–218
  40. Lundby, A., Ravn, L. S., Svendsen, J. H., Hauns, S., Olesen, S. P., and Schmitt, N. (2008) *KCNE3* mutation V17M identified in a patient with lone atrial fibrillation. *Cell. Physiol. Biochem.* **21**, 47–54
  41. Nakajima, T., Wu, J., Kaneko, Y., Ashihara, T., Ohno, S., Irie, T., Ding, W. G., Matsuura, H., Kurabayashi, M., and Horie, M. (2012) *KCNE3* T4A as the genetic basis of Brugada-pattern electrocardiogram. *Circ. J.* **76**, 2763–2772
  42. Ohno, S., Toyoda, F., Zankov, D. P., Yoshida, H., Makiyama, T., Tsuji, K., Honda, T., Obayashi, K., Ueyama, H., Shimizu, W., Miyamoto, Y., Kamakura, S., Matsuura, H., Kita, T., and Horie, M. (2009) Novel *KCNE3* mutation reduces repolarizing potassium current and associated with long QT syndrome. *Hum. Mutat.* **30**, 557–563
  43. Zhang, D. F., Liang, B., Lin, J., Liu, B., Zhou, Q. S., and Yang, Y. Q. (2005) [*KCNE3* R53H substitution in familial atrial fibrillation]. *Chin. Med. J. (Engl.)* **118**, 1735–1738

Received for publication August 31, 2016.

Accepted for publication March 13, 2017.



## Targeted deletion of *Kcne3* impairs skeletal muscle function in mice

Elizabeth C. King, Vishal Patel, Marie Anand, et al.

*FASEB J* 2017 31: 2937-2947 originally published online March 29, 2017

Access the most recent version at doi:[10.1096/fj.201600965RR](https://doi.org/10.1096/fj.201600965RR)

---

**Supplemental Material** <http://www.fasebj.org/content/suppl/2017/03/29/fj.201600965RR.DC1>

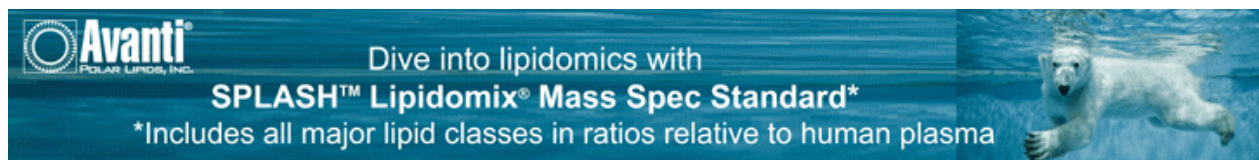
**References** This article cites 41 articles, 14 of which can be accessed free at:  
<http://www.fasebj.org/content/31/7/2937.full.html#ref-list-1>

**Subscriptions** Information about subscribing to *The FASEB Journal* is online at  
<http://www.faseb.org/The-FASEB-Journal/Librarian-s-Resources.aspx>

**Permissions** Submit copyright permission requests at:  
<http://www.fasebj.org/site/misc/copyright.xhtml>

**Email Alerts** Receive free email alerts when new an article cites this article - sign up at  
<http://www.fasebj.org/cgi/alerts>

---



**Avanti**  
POLAR LIPIDS, INC.

Dive into lipidomics with  
**SPLASH™ Lipidomix® Mass Spec Standard\***

\*Includes all major lipid classes in ratios relative to human plasma

Gene name	Fold-change	P value	Gene name	Fold-change	P value
<i>Kcna1</i>	NS	0.94	<i>Kcnk1</i>	NS	0.09
<i>Kcna2</i>	NS	0.08	<i>Kcnk2</i>	NS	0.37
<i>Kcna3</i>	NS	0.14	<i>Kcnk3</i>	NS	0.69
<i>Kcna4</i>	NS	0.51	<b><i>Kcnk4</i></b>	<b>1.2</b>	<b>0.03</b>
<i>Kcna5</i>	NS	0.51	<i>Kcnk5</i>	NS	0.64
<i>Kcna6</i>	NS	0.29	<i>Kcnk6</i>	NS	0.28
<i>Kcna7</i>	NS	0.13	<i>Kcnk7</i>	NS	0.77
<i>Kcna10</i>	NS	0.51	<i>Kcnk9</i>	NS	0.06
<i>Kcnb1</i>	NS	0.14	<i>Kcnk10</i>	NS	0.27
<i>Kcnb2</i>	NS	0.58	<i>Kcnk12</i>	NS	0.36
<i>Kcnc1</i>	NS	0.28	<i>Kcnk13</i>	NS	0.42
<i>Kcnc2</i>	NS	0.44	<i>Kcnk15</i>	NS	0.55
<i>Kcnc3</i>	NS	0.91	<i>Kcnk16</i>	NS	0.09
<b><i>Kcnc4</i></b>	<b>-1.4</b>	<b>0.01</b>	<i>Kcnk18</i>	NS	0.15
<i>Kcnd1</i>	NS	0.78	<i>Kcnn1</i>	NS	0.30
<i>Kcnd2</i>	NS	0.89	<i>Kcnn2</i>	NS	0.75
<i>Kcnd3</i>	NS	0.19	<i>Kcnn3</i>	NS	0.51
			<i>Kcnn4</i>	NS	0.41
<i>Kcnh1</i>	NS	0.95	<i>Kcnma1</i>	NS	0.58
<b><i>Kcnh2</i></b>	<b>-1.1</b>	<b>0.01</b>	<i>Kcnmb1</i>	NS	0.34
<i>Kcnh3</i>	NS	0.34	<i>Kcnmb2</i>	NS	0.11
<i>Kcnh4</i>	NS	0.41	<i>Kcnmb3</i>	NS	0.19
<i>Kcnh5</i>	NS	0.62	<i>Kcnmb4</i>	NS	0.17
<i>Kcnh6</i>	NS	0.09			
<i>Kcnh7</i>	NS	0.07			
<i>Kcnh8</i>	NS	0.35			
<i>Kcnj1</i>	NS	0.14	<i>Kcnq1</i>	NS	0.47
<i>Kcnj2</i>	NS	0.76	<i>Kcnq2</i>	NS	0.06
<i>Kcnj3</i>	NS	0.46	<i>Kcnq3</i>	NS	0.71
<i>Kcnj4</i>	NS	0.10	<i>Kcnq4</i>	NS	0.32
<i>Kcnj5</i>	NS	0.22	<i>Kcnq5</i>	NS	0.40
<i>Kcnj6</i>	NS	0.44			
<i>Kcnj8</i>	NS	0.28			
<i>Kcnj9</i>	NS	0.12			
<i>Kcnj10</i>	NS	0.12			
<i>Kcnj11</i>	NS	0.45			
<i>Kcnj12</i>	NS	0.86			
<i>Kcnj13</i>	NS	0.43			
<i>Kcnj14</i>	NS	0.91			
<i>Kcnj15</i>	NS	0.53			
<i>Kcnj16</i>	NS	0.07			

**Supplementary Table 1. K<sup>+</sup> channel transcript expression changes in female *Kcne3*<sup>-/-</sup> mouse gastrocnemius versus *Kcne3*<sup>+/-</sup>.** Transcripts are organized by gene family, not filtered for intensity (all annotated transcripts in microarray are shown). Fold-changes are given only when P<0.05 (otherwise, listed as NS (not significant)).